Out-of-Plane Bending of URM Walls Strengthened with FRP Strips – Modeling and Analysis

by E. Hamed and O. Rabinovitch

Synopsis: The modeling and analysis of un-reinforced masonry walls strengthened with externally bonded unidirectional composite laminates and subjected to out-of-plane loading is investigated. The model is based on variational principles, static equilibrium, and compatibility between the structural components, which include the masonry units (blocks), the mortar joints, the FRP strips, and the adhesive layers. The modeling of the masonry block and the mortar joints follows the small displacements and the Bernoulli-Euler beam theories. The strengthening FRP strips are modeled following the lamination theory and the adhesive layers are modeled as two dimensional linear elastic continuum. The effects of cracking of the mortar joints and the debonding of the composite laminates near the mortar joints are also considered. A numerical example is presented. The numerical results quantitatively describe some of the phenomena that govern the behavior of the strengthened wall and may lead to its failure. A summary and conclusions close the paper.

Keywords: analysis; cracking; debonding; FRP; masonry; out-of-plane bending; strengthening; theoretical modeling

Ehab Hamed is a Ph.D. student at the Faculty of Civil and Environmental Engineering at the Technion – Israel Institute of Technology.

Dr. Oded Rabinovitch is a senior lecturer and Horev fellow at the Faculty of Civil and Environmental Engineering at the Technion – Israel Institute of Technology.

INTRODUCTION

The structural strengthening and upgrading of existing masonry walls has recently gained much attention. One of the reasons that make this task challenging is the vulnerability of the masonry wall to seismic, blast, and wind forces. These forces are associated with in-plane and out-of-plane bending, which may yield loss of functionality, structural damage, injury to residents, and even loss of lives under earthquake events, blast, or explosions (Ehsani, Saadatmanesh, and Velazquez-Dimas 1999). In other cases, upgrading of masonry walls to become load carrying members is required in order to improve the overall resistance of the entire building. For example, masonry walls in buildings that were designed with little or no regard to seismic and wind forces, in-filled masonry frames in "soft stories", masonry walls in structures that exhibit high levels of inter-story drift, and others may require structural strengthening.

Strengthening and upgrading of masonry walls to resist out-of-plane or in-plane bending can be conducted in many ways. Kahn (1984) and Karantoni and Fardis (1992) discussed the application of shotcrete or ferrocement to the outer faces of the wall. Bhende and Ovadia (1994) investigated the addition of steel plates to the face of the wall. Dawe and Aridru (1993) studied the application of external prestressing, and Manzouri et al. (1996) examined the efficiency of filling the interior voids and cracks with grout and the introduction of steel reinforcement into the masonry wall. Although these methods offer a broad range of practical solutions, they are often time consuming. Furthermore, they add significant mass to the structure, encroach upon available working space, and adversely affect the aesthetics of the repaired area (Triantafillou 1998). One solution that overcomes these obstacles is the use of externally bonded composite materials. This technique uses strips, rods, sheets, or fabrics made of composite and fiber reinforced plastic (FRP) materials that provide the existing wall with additional tensile reinforcement (Schwegler 1995, Hamilton and Dolan 2001).

In general, masonry walls subjected to out-of-plane loading fail by bed-joint cracking at midspan followed by a sudden snap and total collapse (Hamoush et al. 2001). The application of the externally bonded composite layers modifies the bending behavior of the wall and converts it into a load carrying member. Experimental investigations have shown that the strength of the wall can be increased by a factor of up to 50 (Gilstrap and Dolan 1998). In addition, while externally bonded composite laminates tend to decrease the ductility of strengthened RC beams, the strengthened masonry wall exhibits a significant increase in ductility (Ghobarah and El Mandooh Galal, 2004).

Based on the experimental studies of Velazquez-Dimas and Ehsani 2000, Hamilton and Dolan 2001, Hamoush et al. 2002, and Kiss et al. 2002, the modes of failure of the strengthened masonry wall include rupture of the FRP strip or crushing of the masonry at

the bed-joints, debonding (delamination) of the FRP composite at the edges and near the bed-joints, shear failure of the masonry blocks, and peeling of the composite near diagonal shear cracks. Additional modes of failure such as outward buckling/wrinkling of the compressed FRP strip (Kuzik, Elwi, and Cheng 2003), out-of-plane sliding of the blocks at the bed-joints (Tumialan, Galati, and Nanni 2003), punching shear under concentrated loads (Tan and Patoary 2004), flexural-shear cracking, and failure of the block between adjacent FRP strips (Albert, Elwi, and Roger Cheng 2001) have also been observed. Most of these modes of failure are unique to the strengthened wall and have not been observed in un-strengthened masonry walls or in other types of strengthened members such as RC beams, plates and slabs. However, in spite of the comprehensive experimental characterization of these effects, it appears that there are still no analytical models that are able to quantitatively describe and explain the behavior of the strengthened wall. The challenge of developing such model is addressed in this paper.

Among the approaches for the structural analysis of the strengthened wall, the strain compatibility approach has been widely used (Hamilton and Dolan 2001; Hamoush et al. 2002). This model provides an acceptable prediction of the ultimate load in cases of flexural failure by FRP rupture or crushing of the masonry blocks. However, the effect of the delamination, local phenomena in the vicinity of the mortar joints, and other modes of failure are beyond its capability. A similar model, which is also based on the strain compatibility approach while limiting the strains in the FRP strip at different loading stages, was proposed by Velazquez-Dimas and Ehsani (2000). The finite element (FE) method was used by Lee at al. (1996) for the analysis of un-strengthened masonry walls. However, the different length scales (thickness of the adhesive layer and the composite layer versus the depth of the masonry blocks), the differences in the order of magnitude of the mechanical properties of the materials involved, and the singularities and stress concentrations in critical locations make the FE analysis of the strengthened wall very complicated and computational effort consuming.

In this study, a model for the out-of-plane bending behavior of un-reinforced masonry walls strengthened with unidirectional composite strips is presented. The objective of the study is to quantitatively describe the out-of-plane bending behavior of the strengthened masonry wall with emphasis on the critical phenomena that have been experimentally observed. The theoretical model derived in the paper adopts a unidirectional (one-way) representation of the strengthened wall, and uses variational principles, static equilibrium, and compatibility requirements between the structural components (masonry units (blocks), mortar, FRP strips, adhesive layers). Each masonry unit is modeled as a Bernoulli-Euler beam with small deformations. The mortar joints are also modeled using a beam theory, but with a unique constitutive model that represents the cracking and the relatively low stiffness of the mortar joints. Following the concepts of the high order approach (Rabinovitch and Frostig 2000), the composite laminates are modeled using the lamination theory and the adhesive layers are modeled as 2D linear elastic continuum with shear and vertical normal rigidities only. The integrity of the wall is achieved by imposing compatibility requirements between the various structural components.

As reflected by many experimental investigations, the bending behavior of unidirectional strengthened masonry walls is characterized by unique phenomena. Among these, this paper focuses on the deformability of the adhesive layer and its influence on the behavior of the strengthened wall; the cracking of the mortar joint; and the development of stress concentrations and debonding near the mortar joints. The localized stress field near the corners of the masonry blocks; the development of compressive stresses in the composite strip; and the ability of the bonded composite strips to convert the masonry wall into a load carrying member are also investigated. The mathematical formulation, which includes the assumptions, the derivation of the equilibrium equations and the boundary/continuity conditions, the compatibility and debonding conditions, the stress and deformation fields of the adhesive layers, and the governing equations, is presented next. A numerical example that investigates the bending behavior of a strengthened masonry wall and examines the capabilities of the proposed model is also presented. A summary and conclusions close the paper.

RESEARCH SIGNIFICANCE

Masonry walls strengthened with composite materials have been widely studied through experimental researches. The small number and the limited capabilities of the theoretical and analytical models that deal with the complex and unique behavior of strengthened masonry walls triggers the development of a more inclusive and rigorous model. Such model would contribute to the understanding of the behavior of this family of strengthened members. This research presents a theoretical model for the out-of-plane bending behavior of strengthened masonry walls. Its significance is in the contribution to the establishment of a theoretical foundation for the understanding of the physical behavior of the strengthened wall and thus to its effective design and safe use.

MATHEMATICAL FORMULATION

The general layout of the strengthened masonry wall and the sign conventions for the coordinates, deformations, loads, stresses, and stress resultants appear in Figure 1. This layout, and especially the boundary conditions and the strengthening using one-way FRP strips, imply that the structural response of the strengthened wall is a unidirectional (one-way) one. Thus, the deformations and stresses in the un-strengthened direction of the masonry wall and their effects on the behavior of the strengthened direction are not considered. The derivation of the mathematical model assumes that the material behavior of the FRP, adhesive, and the masonry blocks is linear elastic. However, it is assumed that the mortar is linear elastic in compression but its tensile strength and stiffness are negligible. In addition, the longitudinal rigidity of the adhesive layer is neglected with respect to the in-plane stiffness of the masonry blocks and the FRP strips.

The assembly of the various components into a whole structure is based on compatibility between the block units and the mortar joints. Perfect bonding is also attributed to the adhesive-masonry and the adhesive-FRP interfaces. However, debonded (delaminated) regions that may form in the vicinity of the mortar joints are considered.

These debonded regions may be a result of two scenarios. The first is due to insufficient leveling of the mortar joints, which results in a potentially imperfect placement of the adhesive near the mortar joints. The second scenario is due to flexural cracking of the mortar or debonding between the mortar and the masonry unit. In this case, the vertically cracked surface cannot transfer shear stresses. Correspondingly, the horizontal shear stresses at the crack tip (i.e. at the mortar-adhesive interface) are also nullified and a localized debonded region is formed. Thus, the debonded interfaces are free of shear stresses and can only transfer vertical normal compressive stresses if vertical contact exists. Finally, it is assumed that the debonded regions exist before loading and do not grow under it, and that the external loads are applied to the block or the mortar only.

The general layout of the wall (Figure1) indicates that the strengthened panel includes two main types of regions: un-strengthened regions near the external supports, and strengthened regions, in which the FRP strips are bonded on both faces of the masonry panel. The strengthened region may include two types of sub-regions, namely a fully bonded sub-region and a debonded sub-region. A further distinction between debonded sub-regions in which vertical contact exists, and debonded sub-regions without such contact, is made. In case vertical contact exists, the delaminated faces can freely slip with respect to each other (thus cannot resist shear stresses), but maintain vertical compatibility and resist vertical normal compressive stresses. In case vertical contact does not exist, the delaminated faces are free of shear and vertical normal stresses.

Variational principle and Kinematic relations

The equilibrium equations and the boundary/continuity conditions for the strengthened masonry panel are derived through the variational principle, which requires that:

$$\delta(U+V)=0 \tag{1}$$

where U is the strain energy, V is the potential of the external loads, and δ is the variational operator. The first variation of the internal strain energy is

$$\begin{aligned}\delta U = &\sum_{1}^{Nb}\int_{V_{block}}\sigma_{xx}^{block}\delta\varepsilon_{xx}^{block}dv_{block}+\sum_{1}^{Nm}\int_{V_{mortar}}\sigma_{xx}^{mortar}\delta\varepsilon_{xx}^{mortar}dv_{mortar}+\int_{V_t}\sigma_{xx}^{t}\delta\varepsilon_{xx}^{t}dv_t+\int_{V_b}\sigma_{xx}^{b}\delta\varepsilon_{xx}^{b}dv_b\\ &+\int_{V_{ta}}(\tau_{xz}^{ta}\delta\gamma_{xz}^{ta}+\sigma_{zz}^{ta}\delta\varepsilon_{zz}^{ta})dv_{ta}+\int_{V_{ba}}(\tau_{xz}^{ba}\delta\gamma_{xz}^{ba}+\sigma_{zz}^{ba}\delta\varepsilon_{zz}^{ba})dv_{ba}\end{aligned} \tag{2}$$

where the superscripts *block, mortar, t, b, ta* and *ba* refer to the block, mortar, top FRP strip, bottom FRP strip, top adhesive layer, and bottom adhesive layer, respectively; σ_{xx}^{i} and ε_{xx}^{i} are the longitudinal normal stresses and strains in the masonry block *(i=block)*, the mortar joint *(i=mortar)*, the upper FRP strip *(i=t)*, and the lower FRP strip *(i=b)*; τ_{xz}^{j} and σ_{zz}^{j} *(j=ta,ba)* are the shear and vertical normal stresses in the upper and lower adhesive layers, respectively, γ_{xz}^{j} and ε_{zz}^{j} *(j=ta,ba)* are the shear angle and the vertical normal strain in the upper and lower adhesive layers, respectively, and *Nb* and *Nm* are the number of the masonry blocks and mortar joints, respectively.

The kinematic relations for the masonry blocks, the mortar joints, and the upper and lower FRP strips independently follow the Bernoulli-Euler assumption and the theory of small displacements as follows:

$$w_i(x,z_i)=w_i(x)\ ;\ u_i(x,z_i)=u_{oi}(x)-z_i w_{i,x}(x)\ ;\ \varepsilon^i_{xx}(x,z_i)=u_{oi,x}(x)-z_i w_{i,xx}(x) \quad (3a,b,c)$$

where w_i and u_{oi} are the vertical and longitudinal displacements at the reference line (mid-height) of the masonry block *(i=block)*, the mortar joint *(i=mortar)*, the upper FRP strip *(i=t)* or the lower FRP strip *(i=b)*, z_i is measured from the mid-height of each component downwards (Figure 1b), and $(\,)_{,x}$ denotes a partial derivative with respect to x.

Since both the masonry blocks and the mortar joints are modeled as Bernoulli-Euler beams, the equilibrium equations in terms of stress resultants and the boundary/continuity conditions for the block regions and the mortar joint regions are the same and the two components differ only in their constitutive behavior. For brevity, the superscripts *(block)* and *(mortar)* appear in Eq. (1) are replaced with the superscript *(c)*, where *(c=block)* refers to regions in which a block is sandwiched between two FRP strips and adhesive layers ("block regions", sections A-A, B-B in Figure 1a), and *(c=mortar)* refers to regions in which the mortar replaces the block ("mortar regions", section C-C in Figure 1a).

The kinematic relations for the adhesive are based on 2D linear elasticity as follows:

$$\varepsilon^j_{zz}(x,z^j_a)=w^j_{a,z}(x,z^j_a) \quad ; \quad \gamma^j_{xz}(x,z^j_a)=u^j_{a,z}(x,z^j_a)+w^j_{a,x}(x,z^j_a) \quad (4a,b)$$

where w^j_a and u^j_a are the vertical and longitudinal displacements of the upper *(j=ta)* and lower *(j=ba)* adhesive layers.

The first variation of the potential of the external loads equals:

$$\delta V=-\int_{x=0}^{x=L}\left((q_z\delta w_c+n_x\delta u_{oc}+m_x\delta w_{c,x}-\sum_{k=1}^{NC}\left(P_k\delta w_c(x_k)+N_k\delta u_{oc}(x_k)+M_k\delta w_{c,x}(x_k)\right)\delta_D(x-x_k)\right)dx \quad (5)$$

where q_z, n_x, m_x are the external distributed loads and moments exerted at the block or at the mortar, respectively, P_k, N_k and M_k are concentrated loads and bending moments at $x=x_k$, δ_D is the Dirac function, and NC is the number of the concentrated loads.

Compatibility and debonding conditions

The compatibility conditions at the fully bonded adhesive-bock, adhesive-mortar, and adhesive-FRP interfaces are

$$w^{ta}_a(x,z^{ta}_a=0)=w_t(x) \quad ; \quad u^{ta}_a(x,z^{ta}_a=0)=u_{ot}(x)-\frac{h_t}{2}w_{t,x}(x) \quad (6a,b)$$

$$w^{ta}_a(x,z^{ta}_a=c^{ta}_a)=w_c(x) \quad ; \quad u^{ta}_a(x,z^{ta}_a=c^{ta}_a)=u_{oc}(x)+\frac{h_c}{2}w_{c,x}(x) \quad (7a,b)$$

$$w^{ba}_a(x,z^{ba}_a=0)=w_c(x) \quad ; \quad u^{ba}_a(x,z^{ba}_a=0)=u_{oc}(x)-\frac{h_c}{2}w_{c,x}(x) \quad (8a,b)$$

$$w^{ba}_a(x,z^{ba}_a=c^{ba}_a)=w_b(x) \quad ; \quad u^{ba}_a(x,z^{ba}_a=c^{ba}_a)=u_{ob}(x)+\frac{h_b}{2}w_{b,x}(x) \quad (9a,b)$$

where h_c ($=h_{block}$ or h_{mortar}), h_t and h_b are the heights of the masonry block, the mortar joint, and the upper and lower FRP strips, respectively, $c_a{}^{ta}$ and $c_a{}^{ba}$ are the thicknesses of the upper and lower adhesive layers, respectively, and z^j_a *(j=ta,ba)* are measured from the upper interface of each adhesive layer downwards, see Figure 1b.

In the debonded sub-regions, the debonded interface cannot transfer shear or vertical tensile stresses. Hence, the requirements of compatible deformations are replaced with the conditions of stress free surfaces. For example, if the upper adhesive-block interface is debonded and vertical contact exists, Eq. (7b) is replaced with:

$$\tau_{xz}^{ta}(x, z_a^{ta} = c_a^{ta}) = 0 \tag{10}$$

while Eq. (7a) remains unchanged. If vertical contact does not exist, both compatibility conditions, Eqs. (7a) and (7b), are replaced with the following stress conditions:

$$\sigma_{zz}^{ta}(x, z_a^{ta} = c_a^{ta}) = 0 \quad ; \quad \tau_{xz}^{ta}(x, z_a^{ta} = c_a^{ta}) = 0 \tag{11}$$

Equilibrium equations

The equilibrium equations for the strengthened (bonded or debonded) regions are formulated using the variational principle (Eqs. 1,2,5), along with the kinematic relations (Eqs. 3,4), and the compatibility requirements (Eqs. 6-11), as follows:

$$N_{xx,x}^{t} + \alpha_{frp}^{t} b_t \tau_{xz}^{ta}(x, z_a^{ta} = 0) = 0 \tag{12}$$

$$N_{xx,x}^{c} - \alpha_c^{t} b_t \tau_{xz}^{ta}(x, z_a^{ta} = c_a^{ta}) + \alpha_c^{b} b_b \tau_{xz}^{ba}(x, z_a^{ba} = 0) = -n_x \tag{13}$$

$$N_{xx,x}^{b} - \alpha_{frp}^{b} b_b \tau_{xz}^{ba}(x, z_a^{ba} = c_a^{ba}) = 0 \tag{14}$$

$$M_{xx,xx}^{t} + \alpha_{frp}^{t} b_t \frac{h_t}{2} \tau_{xz,x}^{ta}(x, z_a^{ta} = 0) + \beta^{t} b_t \sigma_{zz}^{ta}(x, z_a^{t} = 0) = 0 \tag{15}$$

$$M_{xx,xx}^{c} + \alpha_c^{b} b_b \frac{h_c}{2} \tau_{xz,x}^{ba}(x, z_a^{ba} = 0) + \alpha_c^{t} b_t \frac{h_c}{2} \tau_{xz,x}^{ta}(x, z_a^{ta} = c_a^{ta}) + \beta^{b} b_b \sigma_{zz}^{ba}(x, z_a^{ba} = 0) - \beta^{t} b_t \sigma_{zz}^{ta}(x, z_a^{ta} = c_a^{ta}) = -q_z + m_{x,x} \tag{16}$$

$$M_{xx,xx}^{b} + \alpha_{frp}^{b} b_b \frac{h_b}{2} \tau_{xz,x}^{ba}(x, z_a^{ba} = c_a^{ba}) - \beta^{b} b_b \sigma_{zz}^{ba}(x, z_a^{ba} = c_a^{ba}) = 0 \tag{17}$$

$$\tau_{xz,x}^{ta} + \sigma_{zz,z}^{ta} = 0 \tag{18}$$

$$\tau_{xz,z}^{ta} = 0 \tag{19}$$

$$\tau_{xz,x}^{ba} + \sigma_{zz,z}^{ba} = 0 \tag{20}$$

$$\tau_{xz,z}^{ba} = 0 \tag{21}$$

where N_{xx}^{i} and M_{xx}^{i} are the in-plane stress resultant and the bending moment in the masonry block or the mortar (i=c=*block* or *mortar*) , the upper FRP strip (i=t), and the lower FRP strip (i=b), respectively, b_i (i=t,b) is the width of the upper and lower FRP strips, α_i^{j} is a flag (=0 or 1) that reflects the bonding condition at the upper (j=t) and lower (j=b) adhesive-FRP (i=*frp*) and adhesive-block/mortar (i=c) interfaces, respectively, and $\beta_i^{}$ is a flag that reflects the debonding type (with or without contact). The different combinations of the bonding conditions and type, and the corresponding flags are summarized in Table 1. Note that Eqs. (12-21) are valid for both the block region (c=*block*) and the mortar joint region (c=*mortar*). The distinction between the two cases is achieved through the constitutive relations that are discussed next.

Constitutive relations

At the material point level, the constitutive relations for the blocks are:

$$\sigma_{xx}^{block} = E_{block} \varepsilon_{xx}^{block} \tag{22}$$

where E_{block} is the modulus of elasticity of the block. On the other hand, the material behavior of the mortar assumes linear elastic behavior in compression and negligible tensile strength and stiffness. Thus, the material point level constitutive law for the mortar is:

$$\sigma_{xx}^{mortar} = \begin{Bmatrix} E_{mortar}\varepsilon_{xx}^{mortar} & if & \varepsilon_{xx}^{mortar} \le 0 \\ 0 & if & \varepsilon_{xx}^{mortar} > 0 \end{Bmatrix} \tag{23}$$

where E_{mortar} is the modulus of elasticity of the mortar under compression.

At the cross section level, the constitutive relations are determined by introducing the kinematic relations of Eq. (3c) into Eqs. (22, 23), and using the definitions of the in-plane and bending internal stress resultants. Thus, in general, the constitutive laws for the block and the mortar cross section are:

$$N_{xx}^{c} = \int_{A_c} \sigma_{xx}^{c}(z_c)dA_c = A_{11}^{c}u_{o,x} - B_{11}^{c}w_{c,xx} \qquad (c=block/mortar) \tag{24}$$

$$M_{xx}^{c} = \int_{A_c} \sigma_{xx}^{c}(z_c)z_c dA_c = B_{11}^{c}u_{o,x} - D_{11}^{c}w_{c,xx} \qquad (c=block/mortar) \tag{25}$$

where, A_{11}^{c}, B_{11}^{c} and D_{11}^{c} are the extensional, extensional-flexural, and flexural rigidities of the masonry block *(c=block)* or the mortar joint *(c=mortar)*. The rigidities of the block yield the traditional extensional and flexural rigidities of an elastic section as follows:

$$A_{11}^{block} = \int_{-h_{block}/2}^{h_{block}/2} b_{block}E_{block}dz_{block} = EA_{block} \quad ; \quad B_{11}^{block} = \int_{-h_{block}/2}^{h_{block}/2} b_{block}E_{block}z_{block}dz_{block} = 0 \; ; \tag{26a-c}$$

$$D_{11}^{block} = \int_{-h_{block}/2}^{h_{block}/2} b_{block}E_{block}z_{block}^{2}dz_{block} = EI_{block}$$

where b_{block}, EA_{block} and EI_{block} are the width, extensional stiffness, and flexural stiffness of the block section.

In the mortar joint, the negligible tensile strength and stiffness and the combined in-plane and bending tractions resulting from the external load or the composite action of the masonry panel and the FRP strips, require special consideration. The general stress distributions under the combined tractions appear in Figure 2a. Correspondingly, a distinction is made between the case where the thrust line is located within the middle-third of the mortar cross section and the case where it is located out of the of the middle-third, see Figure 2a and Heyman 1996. (A third case in which the mortar joint is fully detached may develop due to external tensile tractions, yet it is unlikely to occur under normal conditions). In the first case, the mortar joint is un-cracked, it is subjected to compressive stresses through its height, and it exhibits a linear elastic behavior. Therefore, the equivalent rigidities are given by Eq. (26) with the subscript (or superscript) "mortar" instead of "block". In case the thrust line is located outside of the middle-third, the mortar joint is cracked and the material points that undergo positive strain do not contribute to the stiffness of the cross section. Thus, the equivalent rigidities take the following form (see Figure 2b):

$$A_{11}^{mortar} = \int_{-h_{mortar}/2}^{z_o^{mortar}} b_{mortar}E_{mortar}dz_{morta} = E_{mortar}b_{mortar}\left(\frac{h_{mortar}}{2} + \varphi z_o^{mortar}\right) \tag{27}$$

$$B_{11}^{mortar} = \int_{-h_{mortar}/2}^{z_o^{mortar}} b_{mortar} E_{mortar} z_{mortar} dz_{mortar} = -\varphi \frac{E_{mortar} b_{mortar}}{2} \left(\left(\frac{h_{mortar}}{2} \right)^2 - \left(z_o^{mortar} \right)^2 \right) \quad (28)$$

$$D_{11}^{mortar} = \int_{z_o^{mortar}}^{h_{mortar}/2} b_{mortar} E_{mortar} z_{mortar}^{\ 2} dz_{mortar} = \frac{E_{mortar} b_{mortar}}{3} \left(\left(\frac{h_{mortar}}{2} \right)^3 + \varphi \left(z_o^{mortar} \right)^3 \right) \quad (29)$$

where b_{mortar} and $z_o^{\ mortar}$ are the width and the height of the compression zone in the mortar cross section, $\varphi=1$ in case the mortar section is locally subjected to axial compression combined with a positive bending moment, and $\varphi=-1$ if it is combined with a negative moment (see Figure 2b,c). The case in which the mortar joint is fully detached implies that the rigidities of the mortar joint are zero and the functionality of the strengthened wall depends on the FRP strips only. In general, the above formulation introduces a level of nonlinearity into the analytical model and requires the employment of nonlinear or iterative tools. Alternatively, the height of the compression zone may be assessed using simplified approaches. One of these approaches is based on the assumption of a linear strain distribution through the height of the entire strengthened section. Other simplified approach (which is adopted in the numerical study presented in this paper following Hasetline and Moore 1981) assumes that the depth of the compressed zone equals 0.2 the height of the mortar joint.

Note that by adopting the equivalent rigidities formulation (Eqs. 27-29) and by selecting the mid-height surface of the blocks as the reference line throughout the entire panel (blocks and mortar joints), the eccentricity of the cracked joints is introduced through the non-vanishing coupling rigidity B_{11}^{mortar}. This approach simplifies the assembly of the blocks and the mortar joints into a heterogeneous panel with a common reference line.

The constitutive relations for the FRP strips adopt the lamination theory and read

$$N_{xx}^i = A_{11}^i u_{oi,x} - B_{11}^i w_{i,xx} \quad ; \quad M_{xx}^i = B_{11}^i u_{oi,x} - D_{11}^i w_{i,xx} \qquad (i=t,b) \quad (30a,b)$$

where A^i_{11}, B^i_{11} and D^i_{11} $(i=t,b)$ are the extensional, extensional-bending, and flexural rigidities (Vinson and Sierakowski 1986) of the upper and lower FRP strips, multiplied by their width. Finally, the constitutive relations for the adhesive are:

$$\sigma_{zz}^j = E_a^j \varepsilon_{zz}^j \quad ; \quad \tau_{xz}^j = G_a^j \gamma_{xz}^j \qquad (j=ta,ba) \quad (31a,b)$$

where E^j_a and G^j_a $(j=ta,ba)$ are the modulus of elasticity and the shear modulus of the upper and lower adhesive layers, respectively. Note that the constitutive relations assigned for the adhesive layer account for its compressibility in the vertical (out-of-plane) direction and its shear deformability. Due to the significantly lower elastic properties of the adhesive (with respect to the adjacent FRP strips, masonry blocks, or even the mortar joints) its deformability affects the structural behavior of the strengthened element and should be considered.

Adhesive layers - stress and displacement fields

The stress and displacement fields of the adhesive layers in the fully bonded regions are derived using Eqs. (18-21), along with the compatibility requirements (Eqs. 6-9) and the kinematic and constitutive relations (Eqs. 4,31), and they take the following form:

$$\tau^j_{xz,z}(x,z^j_a)=\tau^j_{xz}(x)=\tau^j_a \tag{32}$$

$$\sigma^j_{zz}(x,z^j_a)=-\frac{2z^j_a-c^j_a}{2}\tau^j_{a,x}+\frac{\lambda E^j_a(w_j-w_c)}{c^j_a} \tag{33}$$

$$w^j_a(x,z^j_a)=-\frac{z^{j\,2}_a-c^j_a z^j_a}{2E^j_a}\tau^j_{a,x}+\frac{\lambda(w_j-w_c)z^j_a}{c^j_a}+\frac{(1+\lambda)}{2}w_c+\frac{(1-\lambda)}{2}w_t \tag{34}$$

$$u^j_a(x,z^j_a)=\frac{\tau^j_a z^j_a}{c^j_a}+\frac{\tau^j_{a,xx}}{2E^j_a}\left(\frac{z^{j\,3}_a}{3}-c^j_a\frac{z^{j\,2}_a}{2}\right)-\frac{\lambda\left(w_{i,x}-w_{c,x}\right)z^{j\,2}_a}{2c^j_a}$$
$$-\frac{(1+\lambda)}{2}\left(w_{c,x}\left(z^{ba}_a+\frac{h_c}{2}\right)+u_{oc}\right)+\frac{(1-\lambda)}{2}\left(w_{t,x}\left(z^{ta}_a+\frac{h_c}{2}\right)+u_{ot}\right) \tag{35}$$

where $\lambda=-1$ for the upper $(j=t)$ adhesive layer and $\lambda=1$ for the lower $(j=b)$ layer.
The stress fields at the delaminated adhesive layer (with or without contact) are:

$$\tau^j_{xz,z}(x,z^j_a)=\tau^j_{xz}(x)=\tau^j_a=0 \quad ; \quad \sigma^j_{zz}(x,z^j_a)=\frac{\beta^j\lambda E^j_a(w_j-w_c)}{c^j_a} \tag{36,37}$$

Governing equations

The governing equations for the strengthened (fully bonded or debonded) regions are derived using Eqs. (12-21), the constitutive relations (Eqs. 24-31), the compatibility requirements (Eqs. 7b,9b), and the stress and deformation fields of the adhesive layers (Eqs. 32-37). The governing equations are stated in terms of the unknown displacements w_c, w_t, w_b, u_{oc}, u_{ot}, u_{ob}, and shear stresses τ_a^{ta} and τ_a^{ba} as follows:

$$A^t_{11}u_{ot,xx}-B^t_{11}w_{t,xxx}+\alpha^t_{frp}\alpha^t_c b_t\tau^{ta}_a=0 \tag{38}$$

$$A^c_{11}u_{oc,xx}-B^c_{11}w_{c,xxx}-\alpha^t_{frp}\alpha^t_c b_t\tau^{ta}_a+\alpha^b_{frp}\alpha^b_c b_b\tau^{ba}_a=-n_x \tag{39}$$

$$A^b_{11}u_{ob,xx}-B^b_{11}w_{b,xxx}-\alpha^b_{frp}\alpha^b_c b_b\tau^{ba}_a=0 \tag{40}$$

$$D^t_{11}w_{t,xxxx}-B^t_{11}u_{ot,xxx}-\alpha^t_{frp}\alpha^t_c(c^{ta}_a+h_t)\frac{b_t\tau^{ta}_{a,x}}{2}+\beta^t\frac{b_tE^t_a}{c^t_a}(w_t-w_c)=0 \tag{41}$$

$$D^c_{11}w_{c,xxxx}-B^c_{11}u_{oc,xxx}-\alpha^b_{frp}\alpha^b_c(c^{ba}_a+h_c)\frac{b_b\tau^{ba}_{a,x}}{2}-\alpha^t_{frp}\alpha^t_c(c^{ta}_a+h_c)\frac{b_t\tau^{ta}_{a,x}}{2}$$
$$+\beta^b\frac{b_bE^{ba}_a}{c^{ba}_a}(w_c-w_b)-\beta^t\frac{b_tE^{ta}_a}{c^{ta}_a}(w_t-w_c)=-q_z+m_{x,x} \tag{42}$$

$$D^b_{11}w_{c,xxxx}-B^b_{11}u_{oc,xxx}-\alpha^b_{frp}\alpha^b_c(c^{ba}_a+h_b)\frac{b_b\tau^{ba}_{a,x}}{2}-\beta^b\frac{b_bE^{ba}_a}{c^{ba}_a}(w_c-w_b)=0 \tag{43}$$

$$\alpha^t_{frp}\alpha^t_c\left(u_{ot}-u_{oc}-\frac{(c^{ta}_a+h_t)}{2}w_{t,x}-\frac{(c^{ta}_a+h_c)}{2}w_{c,x}+\frac{\tau^{ta}_a c^{ta}_a}{G^{ta}_a}-\frac{\tau^{ta}_{a,xx}(c^{ta}_a)^3}{12E^{ta}_a}\right)=0 \tag{44}$$

$$\alpha^b_{frp}\alpha^b_c\left(u_{oc}-u_{ob}-\frac{(c^{ba}_a+h_b)}{2}w_{b,x}-\frac{(c^{ba}_a+h_c)}{2}w_{c,x}+\frac{\tau^{ba}_a c^{ba}_a}{G^{ba}_a}-\frac{\tau^{ba}_{a,xx}(c^{ba}_a)^3}{12E^{ba}_a}\right)=0 \tag{45}$$

Note that Eqs. (44) and (45) result from the compatibility conditions of the longitudinal deformations at the upper and lower adhesive layers (Eqs. 7b, 9b). Thus, they exist in the

fully bonded sub-regions and vanish in the debonded ones. Likewise, the corresponding shear stresses, which are uniform through the thickness of each adhesive layer (see Eq. 32), also vanish in the debonded sub-regions and are not considered as unknowns. The distinction between the block and mortar regions (both governed by Eqs. 38-45) is made through the different elasto-geometric (rigidities) properties of the two regions (see Eqs. 26-29). For simplicity, it is assumed that due to the relatively small length of the mortar joint, these elasto-geometric properties are uniform through the length of the joint. The link between the various sub-regions (block, mortar, bonded, debonded, etc.) is achieved through the continuity conditions that are discussed next.

Continuity conditions

The continuity conditions at any point $x=x_k$ within the fully bonded sub-region are:

$$u_{oi}^{(-)} = u_{oi}^{(+)} \quad ; \quad w_i^{(-)} = w_i^{(+)} \quad ; \quad w_{i,x}^{(-)} = w_{i,x}^{(+)} \quad ; \quad w_a^{j(-)}(z_a^j) = w_a^{j(+)}(z_a^j) \quad (i=c,t,b) \qquad (46a\text{-}d)$$

$$N_{xx}^{i(-)} - N_{xx}^{i(+)} = \kappa N_k^i \qquad (i=c,t,b) \qquad (47)$$

$$\left(M_{xx,x}^{i(-)} + (1-\kappa) b_i h_i \tau_a^{i(-)} + \kappa \frac{h_c}{2} (b_t \tau_a^{t(-)} + b_b \tau_a^{b(-)}) - \kappa m_x^{(-)} \right) \qquad (i=c,t,b) \qquad (48)$$

$$- \left(M_{xx,x}^{i(+)} + (1-\kappa) b_i h_i \tau_a^{i(+)} + \kappa \frac{h_c}{2} (b_t \tau_a^{t(+)} + b_b \tau_a^{b(+)}) - \kappa m_x^{(+)} \right) = \kappa P_k$$

$$- M_{xx}^{i(-)} + M_{xx}^{i(+)} = \kappa M_k^i \qquad (i=c,t,b) \qquad (49)$$

$$\tau_a^{j(-)} = \tau_a^{j(+)} \qquad (i=c,t,b) \qquad (50)$$

where the *(-)* and *(+)* superscripts denote quantities left and right to the point $x=x_k$, respectively, and P_k, N_k and M_k are concentrated loads and bending moments at $x=x_k$. If the connection point $x=x_k$ is located within a debonded sub-region, the continuity conditions include Eqs. (46a-c,47,49) and Eq. (48) after dropping the terms that include the vanishing shear stress.

The continuity conditions at the connection points between the fully bonded sub-region and the debonded sub-region include Eqs. (46a-c,47-49) after dropping the vanishing shear stress at the debonded sub-region, and an additional condition that is applied only to the fully bonded sub-region. This condition requires that the shear stress, which is unknown only in the fully bonded region, equals zero at the connection point.

For brevity, the boundary conditions are not explicitly presented here. However, they can be obtained by degenerating the continuity conditions and selecting either a kinematic condition or a static one (i.e. Eq. 46a or 47, Eq. 46b or 48, Eq. 46c or 49, Eq. 46d or 50).

The governing equations of the various regions along with the boundary and continuity conditions are numerically solved using the Multiple Shooting method (Stoer and Bulirsch 1993). The determination of the type of debonded sub-regions (with or without contact) is conducted iteratively. Namely, one type is assumed and verified through the results of the analysis. If the results contradict the assumption, the assumed type of the debonded region is switched and the structure is re-analyzed.

NUMERICAL STUDY

The bending behavior of a masonry panel strengthened with unidirectional GFRP strips bonded to its upper and lower faces is investigated. The geometry, mechanical properties, and the lateral loads (self weight and two concentrated loads) follow the experimental study of Kiss et al. (2002) and appear in Figure 3. Two cases of bonding conditions are considered. At first, the FRP strips are assumed to be fully bonded through the length of the masonry panel. The second case assumes that debonded regions exist through the length of the mortar joints, plus a distance that is estimated as twice the thickness of the adhesive layer (see Figure 3c). These effects are considered in order to describe the behavior of the strengthened masonry wall at progressive levels of load, where cracking of the mortar joint, debonding between the mortar and the masonry unit, or potentially imperfect placement of the adhesive near the mortar joints may trigger the development of such debonded regions.

The response of the fully bonded masonry wall in terms of the deformations, internal forces, and stresses in the adhesive layers is described in Figure 4. The results show the slope change of the deflection line at the mortar joints (Figure 4a). They also show the amplified longitudinal deformations through the length of the joint (Figure 4b). This effect is attributed to cracking of the mortar and to its relative deformability. However, while the un-strengthened masonry wall fails after progressive cracking of one mortar joint near mid-span, the strengthened wall allows the development of cracks in more than one mortar joint along the wall. This effect, which is detected by the analysis, provides the strengthened wall with the ability to resist bending moments beyond the cracking point, by composite action in terms of axial forces in the masonry panel and the FRP strips.

Figures 4c and 4d quantitatively show that the reduced flexural stiffness of the mortar joints yield a reduction in the localized bending moment carried by the wall, and a corresponding increase in the axial tensile/compressive forces in the FRP strips and the wall. The shear forces distribution (see Figure 4e) shows that although the global shear force is null between the two concentrated loads ($380<x<520$ *mm*), self equilibrated shear forces develop in the masonry panel due to localized effects near the mortar joints. These localized effects are also observed in the distribution of the shear and vertical normal (peeling) stresses in the adhesive layers near the mortar joints (see Figure. 4f,g,h). The stress concentrations observed in these figures provide a quantitative explanation of the debonding failure mechanism that has been observed in experimental studies (Hamilton and Dolan 2001; Kiss et al. 2002). Peeling stress concentrations are also observed at the edges of the FRP strips, and explain the edge debonding failure that was also experimentally observed (Hamoush et al. 2001; Hamoush et al. 2002).

The distribution of the peeling stresses in the adhesive layers near the mortar joint at mid-span appears in Figure 5. The curves for the lower adhesive interfaces reveal that the adhesive-block interface is subjected to compression stresses at the edges of the mortar joint. These stresses result from the vertical interaction of the corners of the block, the adhesive layer, and the FRP strip. In other words, the lower corners of the masonry blocks are compressed against the FRP strip. On the other hand, the upper corners of the

blocks pull the upper FRP strip downwards, result in the formation of tensile vertical stresses at the adhesive-block interface, and may lead to debonding failure. Within the mortar joint itself, the stresses at the adhesive-mortar interface diverge from the stresses at the adhesive FRP one. This effect is attributed to the shear gradient terms that appear in the vertical normal stress fields (Eq. 33). Yet, the average stresses through the thickness, which equal the stresses at $z^j_a = c^j_a /2$ and result from the vertical deformability of the adhesive (see Eq. 33), clarify that the FRP strips are compressed against the lower face of the joint and pulled down by the upper face. In both cases, the localized effects and stress concentrations as well as the cracking of the mortar material probably lead to debonding. The response of the structure under these conditions is examined next.

The response of the debonded masonry wall in terms of the vertical deflections and internal axial forces appear in Figure 6. The results show that the formation of the debonded regions decreases the flexural rigidity of the masonry wall and increases its vertical deflections. The distribution of the axial forces in the wall and the FRP strips reveals that the upper FRP strip is subjected to compression forces. These compression forces and the reduced or vanished lateral support of the adhesive layer may lead to local buckling of the strip and to further propagation of the debonded region (Rabinovitch 2004a)

The distribution of the shear and the vertical normal stresses in the adhesive layers in the vicinity of the mortar joint at mid-span is described in Figure 7. These results show that the formation of the debonded regions significantly increases the magnitudes of the shear and vertical normal stresses (see Figures 4f,g,h and 7). It is also seen that the magnitudes of these stresses are far beyond the strength of the cementicious materials involved and may lead to a localized or overall debonding failure. This failure mechanism, which is quantitatively characterized here has been observed in many experimental studies (see Kiss et al. 2002; Kuzik et al. 2003; Tumialan et al. 2003). Furthermore, the results presented in Figure 7 can be used for the evaluation of a fracture mechanics criterion for the propagation of the debonding failure (Rabinovitch and Frostig 2001, Rabinovitch 2004b).

SUMMARY AND CONCLUSIONS

A theoretical approach for the description of the out-of-plane bending behavior of un-reinforced masonry walls strengthened with unidirectional composite strips has been presented. The structural high order model is based on variational principles, static equilibrium, and compatibility requirements between the structural components (masonry blocks, mortar, FRP strips, adhesive layers). The Bernoulli-Euler beam assumptions and the theory of small displacements have been adopted for the modeling of the masonry blocks and the mortar joints. The strengthening composite laminates have been modeled using the lamination theory, and the adhesive layers have been considered as 2D linear elastic continua. Compatibility requirements at the interfaces of the adhesive layers and at the connection points between the various structure components have been used to assemble the various components into a whole structure.

The capabilities of the proposed approach have been examined through a numerical example. It has been shown that as expected and aimed by the strengthening process, the behavior of the strengthened masonry wall is similar to the behavior of a reinforced masonry wall, where cracks can develop in more than one critical mortar joint. This effect is well predicted by the analytical model. The numerical study has shown that the proposed model quantitatively describes the localized interaction between the FRP strips and the corners of the masonry block. This effect may lead to local shear failure of the FRP strips, and thus have to be considered in the design of strengthened masonry walls. The results have also revealed the development of high shear and vertical normal (peeling) stresses in the adhesive layers at the vicinity of the mortar joints as well as at the edges of the FRP strips. These stress concentrations provide a quantitative explanation of the debonding failure that has been observed in many experimental studies. In addition, the numerical study has quantitatively characterized the development of compressive forces in the upper FRP strip. This effect may lead to buckling or local wrinkling of the FRP strip, especially at the debonded zones near the mortar joints.

In conclusion, it is seen that the bending behavior of strengthened masonry walls is characterized by unique aspects that have not been observed in the un-strengthened wall or in other strengthened members. This study throws light on some of these aspects and sets a basis for further investigations of this unique structural member. Topics for ongoing and future investigation of strengthened URM walls include a detailed parametric study with emphasis on variables that are prescribed by the given properties of the wall (dimensions, materials, slenderness ratio, construction method, boundary conditions, etc.), and parameters that can be controlled by the designer of the strengthening system (FRP and adhesive materials and geometry, strengthening scheme, etc.). An enhancement of the analytical model to account for nonlinear effects that evolve at the higher load levels and a detailed comparison to experimental data are also under investigation. Finally, the challenge of developing a practical design protocol based on the theoretical tools and information gathered in the study is also considered for future research.

REFERENCES

Albert, M.L., Elwi, A.E., and Cheng, J.J.R., 2001, “Strengthening of Unreinforced Masonry Walls using FRPs”, *Journal of Composite for Construction*, Vol. 5, No. 2, pp. 76-84.

Bhende, D. and Ovadia, D. 1994, “Out-of-Plane Strengthening Scheme for Reinforced Masonry Walls” *Concrete International* Vol. 16, No. 4, pp. 30-34.

Dawe, J.L. and Aridru, G.G., 1993, “Prestressed Concrete Masonry Walls Subjected to Uniform Out-of-Plane Loading”, *Canadian Journal of Civil Engineering*, Vol. 20, No. 6, pp. 969-979.

Ehsani, M.R., Saadatmanesh, H. and Velazquez-Dimas, J.I., 1999, “Behavior of Retrofitted URM Walls Under Simulated Earthquake Loading”, *Journal of Composites for Construction*, Vol. 3, No. 3, pp. 134-142.

Ghobarah, A. and El Mandooh Galal, K., 2004, "Out-of-Plane Strengthening of Unreinforced Masonry Walls with Openings", *Journal of Composites for Construction*, Vol. 8, No. 4, pp. 298-305.

Gilstrap, J.M. and Dolan, C.W., 1998, "Out-of-plane Bending of FRP-Reinforced Masonry Walls", *Composites Science and Technology*, Vol. 58, No. 8, pp. 1277-1284.

Hamilton, H.R. and Dolan, C.W., 2001, "Flexural Capacity of Glass FRP Strengthened Concrete Masonry Walls", *Journal of Composites for Construction*, Vol. 5, No. 3, pp. 170-178.

Hamoush, S.A., McGinley, M.W., Mlakar, P., Scott, D. and Murray, K., 2001, "Out-of-Plane Strengthening of Masonry Walls with Reinforced Composites", *Journal of Composites for Construction*, Vol. 5, No. 3, pp. 139-145.

Hamoush, S.A., McGinley, M.W., Mlakar, P., Terro, M.J., 2002, "Out-of-Plane Behavior of Surface-Reinforced Masonry Walls", *Construction and Building Materials*, Vol. 16, No. 6, pp. 341-351.

Hasetline, B.A. and Moore, J.F.A., 1981, *Handbook to BS5628: Structural use of Masonry, Part1: Unreinforced Masonry*. Brick Development Association Windsor, U.K

Heyman, J., 1996, *Arches, Vaults, and Buttresses.* Variorum, Ashgate Publishing company, Brookfiled, Vermont, USA.

Kahn, L.F., 1984, "Shotcrete Strengthening of Brick Masonry Walls", *Concrete International: Design and Construction*, Vol. 6, No. 7, pp. 34-39.

Karantoni, F.V. and Fardis, M.N., 1992, "Effectiveness of Seismic Strengthening Techniques for Masonry Buildings", *Journal of Structural Engineering*, Vol. 118, No. 7, pp. 1884-1902.

Kiss, R.M., Kollar, L.P., Jai, J. and Krawinkler, H., 2002, "Masonry Strengthened with FRP Subjected to Combined Bending and Compression, Part II: Test Results and Model Predictions", *Journal of Composite Materials*, Vol. 36, No. 9, pp. 1049-1063.

Kuzik, M.D., Elwi, A.E. and Cheng, J.J.R., 2003, "Cyclic Flexure Tests of Masonry Walls Reinforced with Glass Fiber Reinforced Polymer Sheets", *Journal of Composite for Construction*, Vol. 7, No. 1, pp. 20-30.

Lee, J.S., Pande, G.N., Middleton, J. and Kralj, B., 1996, "Numerical Modeling of Brick Masonry Panels Subject to Lateral Loading", *Computers and Structures*, Vol. 61, No. 4, pp. 735-745.

Manzouri, T., Schuller, M.P., Shing, P.B. and Amadei, B., 1996, "Repair and Retrofit of Unreinforced Masonry Structures", *Earthquake Spectra*, Vol. 12, No. 4, pp. 903-922.

Rabinovitch, O., 2004a, "Nonlinear (Buckling) Effects in RC Beams Strengthened with Composite Materials Subjected to Compression". *International Journal of Solids and Structures*, vol. 41, No. 20, pp. 5677-5695.

Rabinovitch, O., 2004b, "Fracture-Mechanics Failure Criteria for RC Beams Strengthened with FRP Strips - a Simplified Approach". *Composite Structures*, vol. 64, No. 3-4, pp. 479-492.

Rabinovitch, O. and Frostig, Y., 2000, "Closed-Form High-Order Analysis of RC Beams Strengthened with FRP Strips" *Journal of Composites for Construction*, Vol. 4, No. 2, pp. 65-74.

Rabinovitch, O. and Frostig, Y., 2001, "Delamination Failure of RC Beams Strengthened with FRP Strips – A Closed-Form High-Order and Fracture Mechanics Approach", *Journal of Engineering Mechanics*, Vol. 127, No. 8, pp. 852-861.

Schwegler, G., 1995, "Masonry Construction Strengthened with Fiber Composites in Seismically Endangered Zones". *10th European Conference on Earthquake Engineering*, Duma (Ed.), Balkema, Rotterdam, pp. 2299-2303.

Tan, K.H. and Patoary, M.K.H., 2004, "Strengthening of Masonry Walls against Out-of-Plane Loads using Fiber-Reinforced Polymer Reinforcement", *Journal of Composites for Construction*, Vol. 8, No. 1, pp. 79-87.

Triantafillou T.C., 1998a, "Strengthening of Masonry Structures using Epoxy-Bonded FRP Laminates", *Journal of Composites for Construction*, Vol. 2, No. 2, pp. 96-104.

Tumialan, J.G., Galati, N. and Nanni, A., 2003, "Fiber-Reinforced Polymer Strengthening of Unreinforced Masonry Walls Subjected to Out-of-Plane Loads", *ACI Structural Journal,* Vol. 100, No. 3, pp. 321-329.

Velazquez-Dimas, J.I. and Ehsani, M.R., 2000, "Modeling Out-of-Plane Behavior of URM Walls Retrofitted with Fiber Composites", *Journal of Composites for Construction*, Vol. 4, No. 4, pp. 172-181.

Vinson, J. R. and Sierakowski, R. L., 1986, *The Behavior of Structures Composed of Composite Materials*, Martinus-Nijhoff, Inc., Dordrecht, The Netherlands

Table 1 – Values of the α_i^j and β^j flags corresponding to the bonding conditions and type of delamination at the interfaces of the adhesive layers.

i	*j*	Location	Condition	α_i^j	β^j
frp	*t*	upper adhesive-FRP interface	Bonded	1	1
			Debonded with contact	0	1
			Debonded without contact	0	0
c	*t*	upper adhesive-block/mortar interface	Bonded	1	1
			Debonded with contact	0	1
			Debonded without contact	0	0
frp	*b*	lower adhesive-FRP interface	Bonded	1	1
			Debonded with contact	0	1
			Debonded without contact	0	0
c	*b*	lower adhesive-block/mortar interface	Bonded	1	1
			Debonded with contact	0	1
			Debonded without contact	0	0

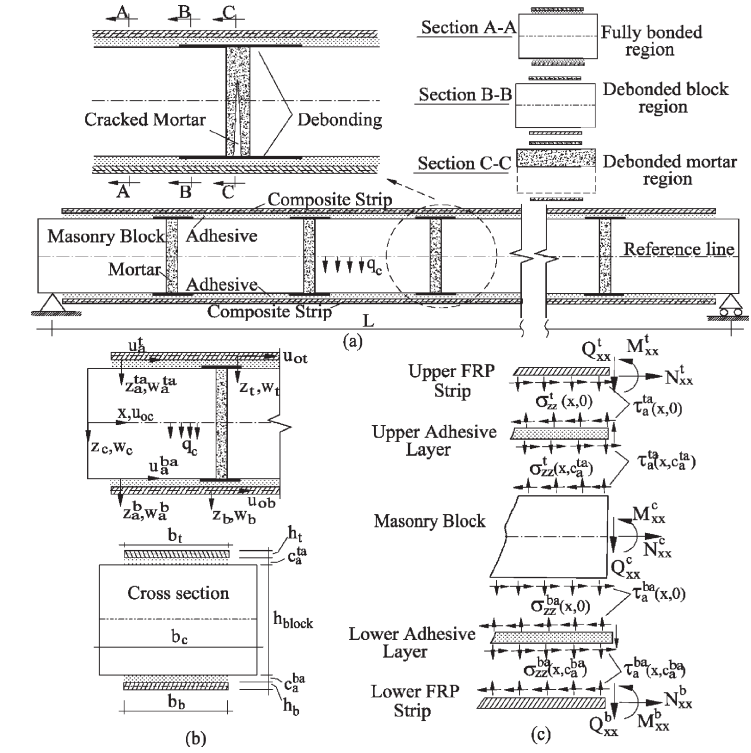

Figure 1 – Geometry, loads, sign conventions, and stress resultants: (a) Geometry and loads; (b) Coordinate systems and deformations; (c) Stresses and stress resultants.

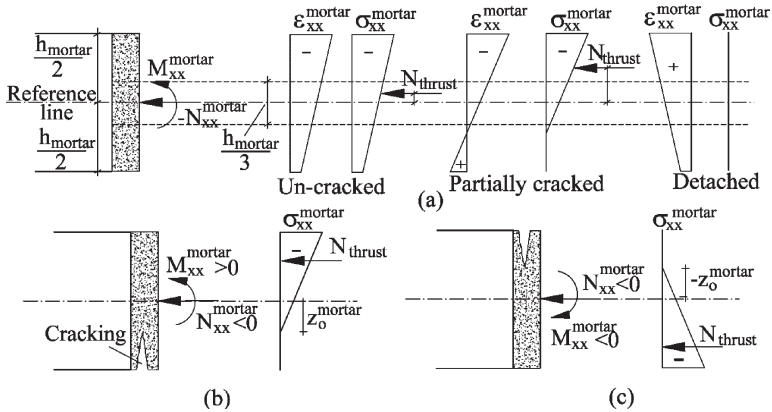

Figure 2 – Stress distributions through the height of the mortar joint: (a) influence of the location of thrust line; (b) Stress distribution in cracked mortar joint subjected to positive moment and axial compressive force; (c) Stress distribution in cracked mortar joint subjected to negative moment and axial compressive force.

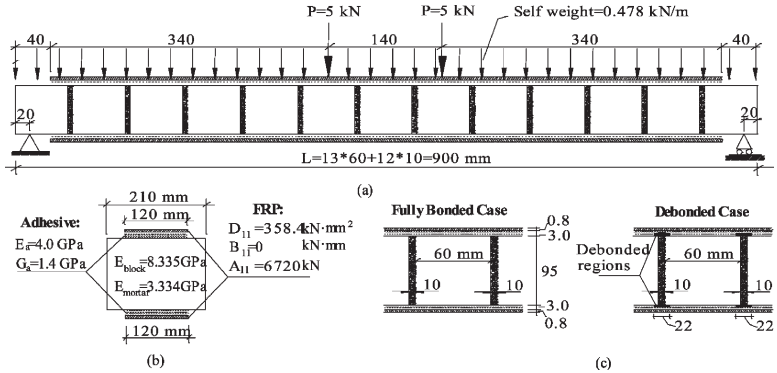

Figure 3 – Geometry, material properties, and load pattern: (a) Geometry and loading scheme; (b) Cross section and mechanical properties; (c) Full bonded and debonded case of the FRP strips near the mortar joints.

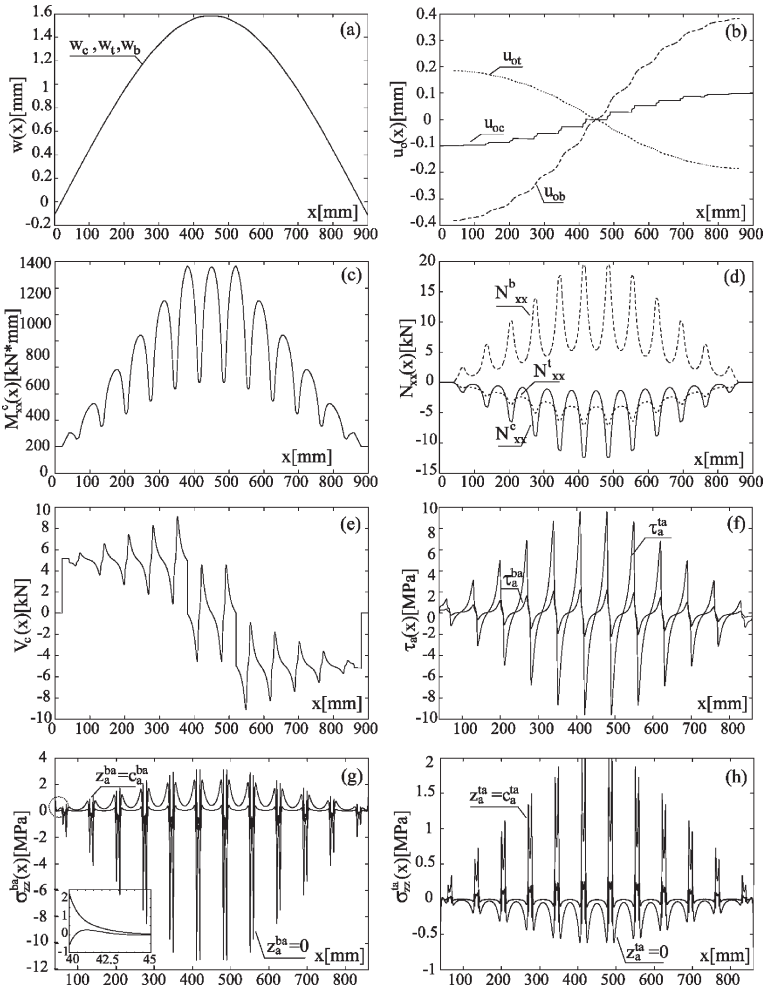

Figure 4 – Response of the fully bonded strengthened wall: (a) Vertical deflections; (b) Longitudinal deformations; (c) Bending moment in the wall; (d) Axial forces; (e) Shear forces in the wall; (f) Shear stresses at the adhesive layers; (g) Vertical normal stresses at the lower adhesive layer; (h) Vertical normal stresses at the upper adhesive layer.

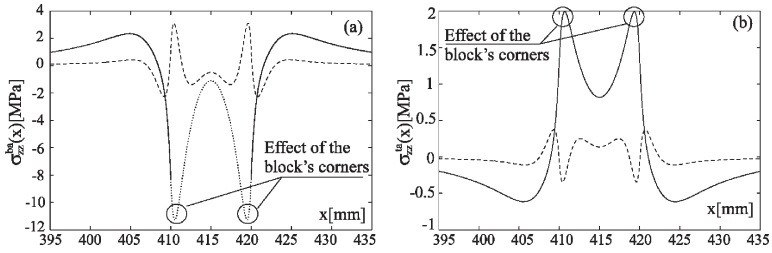

Figure 5 – Vertical normal stresses in the adhesive at the critical mortar joint (at mid-span) – fully bonded case: (a) Stresses at the lower adhesive layer; (b) Stresses at the upper adhesive layer. (Legend: — Adhesive-block interface, ····Adhesive-mortar interface,— Adhesive-FRP interface)

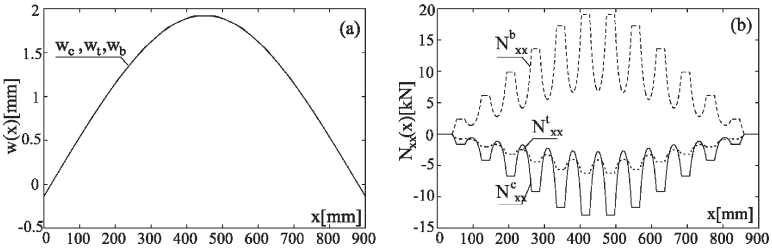

Figure 6 – Response of the wall debonded near the mortar joints: (a) Vertical deflections; (b) Axial forces.

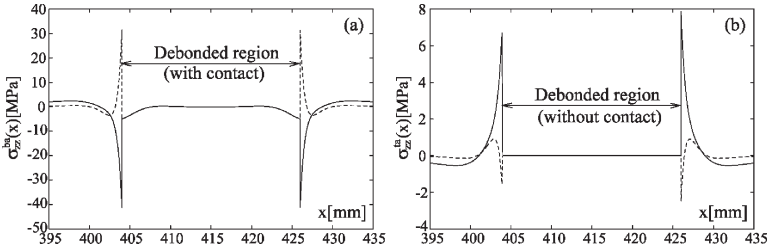

Figure 7 – Vertical normal stresses in the adhesive near the critical joint at mid-span – debonded wall: (a) Stresses at the lower adhesive layer; (b) Stresses at the upper adhesive layer. (Legend: –– Adhesive-block/ mortar interface, — Adhesive-FRP interface.)